These requirements are not exactly fulfilled when the monovalent ions are used. Although in our systems we did not observe very large deviations as observed previously,[21] we consider the Mg^{2+} results more reliable.

Acknowledgment. We are indebted to S. Baer for helpfull discussions. This work was supported by the Israel-USA BNSF and by the Balfour Foundation, Israel.

Registry No. PSS, 9080-79-9; PVS, 25191-25-7; PAA, 9003-01-4; $Ru(bpy)_3^{2+}$, 15158-62-0; $K_4Fe(CN)_6$, 13943-58-3; $MgSO_4$, 7487-88-9; KCl, 7447-40-7; NaCl, 7647-14-5.

References and Notes

(1) Klotz, I. M.; Walker, F. M.; Pivan, R. B. *J. Am. Chem. Soc.* **1946**, *68*, 1486.
(2) Nemethy, G.; Scheraga, H. A. *J. Phys. Chem.* **1962**, *66*, 1773.
(3) Gregor, H. P.; Frederick, M. J. *Polym. Sci.* **1957**, *23*, 451.
(4) Turro, N. J.; Pierola, I. F. *J. Phys. Chem.* **1983**, *87*, 2420.
(5) Miyamoto, S. *Macromolecules* **1981**, *14*, 1054.
(6) Chen, C.-H.; Berns, D. S. *J. Phys. Chem.* **1977**, *81*, 125.
(7) Ben-Naim, A. *Topics in Molecular Pharmacology*; Burgan, A. S. V., Roberts, G. C. K., Eds.; Elsevier: Amsterdam, 1983.
(8) Paramauro, E.; Pelizzetti, E.; Dickmann, S.; Frahm, J. *Inorg. Chem.* **1982**, *21*, 2432.
(9) Webber, S. E. *Macromolecules* **1986**, *19*, 1658.
(10) Morishima, Y.; Kobayashi, T.; Nozakura, S. I. *J. Phys. Chem.* **1985**, *89*, 4081.
(11) Morishima, Y.; Kitani, T.; Kobayashi, T.; Saeki, Y.; Nozakura, S. I.; Ohno, T.; Kato, S. *Photochem. Photobiol.* **1985**, *42*, 457.
(12) Morishima, Y.; Itoh, Y.; Nozakura, S.-I.; Ohno, T.; Kato, S. *Macromolecules* **1984**, *17*, 2264.
(13) Itoh, Y.; Morishima, Y.; Nozakura, S. *J. Polym. Sci., Polym. Chem. Ed.* **1982**, *20*, 467.
(14) Morishima, Y.; Itoh, Y.; Nozakura, S.-I. *Chem. Phys. Lett.* **1982**, *91*, 258.
(15) Kurimura, Y.; Yokota, H.; Shigehara, K.; Tsuchida, E. *Bull. Chem. Soc. Jpn.* **1982**, *55*, 55.
(16) Sassoon, R. E.; Gershuni, S.; Rabani, J. *J. Phys. Chem.* **1985**, *89*, 1937.
(17) Lougnot, D.; Dolan, G.; Goldstein, C. R. *J. Phys. E.* **1979**, *12*, 1051.
(18) Breslow, D.; Kutner, K. *J. Polym. Sci.* **1958**, *27*, 295.
(19) Jonah, C. D.; Matheson, M. S.; Meisel, D. *J. Phys. Chem.* **1979**, 83, 257.
(20) Juris, A.; Gandolfi, M. T.; Manfrine, M. F.; Balzani, V. *J. Am. Chem. Soc.* **1976**, *98*, 1047.
(21) Jonah, C. D.; Matheson, M. S.; Meisel, D. *J. Phys. Chem.* **1977**, *81*, 1805.
(22) Ise, N. *J. Polym. Sci., Polym. Symp.* **1978**, *62*, 205.
(23) Fendler, J. H.; Fendler, E. J. *Catalysis in Micellar and Macromolecular Systems*; Academic: New York, 1975.

Whole-Pattern Approach to Structure Refinement Problems of Fibrous Materials. Application to Isotactic Polypropylene

A. Immirzi* and P. Iannelli

Dipartimento di Fisica, Università di Salerno, I-84100 Salerno, Italy.
Received February 25, 1987; Revised Manuscript Received September 18, 1987

ABSTRACT: Following up an idea developed in a previous paper, the crystal structure of the α form of isotactic polypropylene (IPP) has been refined by a least-square fitting procedure by using X-ray diffraction fiber data and considering the fiber spectrum as a whole. This approach represents an extension of the Rietveld method from the one-dimensional case (powders) to a two-dimensional case (fibers). In spite of structure complexity, low resolution, and reflection overlap, well-distinguishable fits have been obtained by considering the two structure models $P2_1/c$ and $C2/c$ which are very closely related to each other. A reliable chain model of 3_1 symmetry was obtained having C–C–C chain angles of 116.9 and 112.4°, chain torsion angles of 178 and 59°, and methyl-to-chain valence angles of 108.2°.

Introduction

In a preceding paper[1] we have discussed the possibility of performing crystal structure refinements from fiber diffraction data by using, instead of "integrated" diffraction intensities, the "whole diffraction pattern", so extending the Rietveld's method[2,3] from the powder to the fiber case. The diffraction pattern as a whole can be digitized by using the photographic technique and a photoscan instrument.

The advantage of the whole-pattern method against the traditional one is that the problem of reflection overlap is removed. Although in fibers overlap is less troublesome than in powders since it takes place only within each layer line, large lattice constants, low symmetry, and wide peak broadening make the problem serious. In the present case, for instance, from 4 to 8 reflections do contribute for at least 20% of their maximum weight to the equatorial points between $\vartheta = 25°$ and $\vartheta = 35°$ (twice as many in the upper level lines), and yet above $\vartheta = 10°$ there are no points without any contribution. Among the overlapped reflections, of course, only a few are "intense"; for a quantitative treatment it is important, however, to consider *all* reflections, not only the intense.

In order to implement fiber whole-pattern refinement procedures, it is necessary to choose suitable profile functions for expressing the distribution of diffracted intensity. While in the powder case a one-variable function is needed (the profile versus the diffraction Bragg angle 2ϑ), in the fiber case two-variable functions are required. In a preceding article[1] we have shown that in the case of the α form of isotactic polypropylene (IPP), X-ray radiation and photographic technique, Gaussian profile functions are adequate for expressing the intensity distribution both in the increasing Bragg angle direction and for a constant Bragg angle direction. On this basis a whole-pattern structure refinement for the same polymer has been carried out by considering, alternatively, the $C2/c$ structural model by Natta and Corradini[4] and the $P2_1/c$ model by Mencick.[5] The two fits are compared and discussed in this paper.

In the present study we have also combined the fiber whole-pattern approach with constrained refinement so considerably reducing the number of structural unknowns. The procedure applied is closely related to that used in powder whole-pattern studies.[6-9]

Experimental Section

The sample of IPP used in this study (the same used in the former work[1]) was stretched at 140 °C and annealed at 140 °C for 3 h. The X-ray fiber diffraction pattern (Cu Kα radiation)

0024-9297/88/2221-0768$01.50/0

was recorded in the present case on a cylindrical camera (radius 28.65 mm) instead of a flat camera in order to achieve higher intensities at the higher diffraction angles. Owing to the wide intensity range, four distinct spectra were recorded with exposures in the ratios 1, 2.67, 10.7, 42.7. Each film (Eastman Kodak DEF-5) was digitized by a photoscan instrument (Optronics System P-1000, Model 30D) according to a 100 × 100 μm grid. The four data files so obtained were merged into a single data file by considering appropriate "windows" in the diffraction pattern and taking for each window the film having the highest optical density within the linearity range. Each optical density measurement was converted in energy per unit area E_{obsd} by subtracting the fixed value due to optical absorption of the film base (estimated separatedly from a calibration film) and taking into account that diffracted beams incide obliquely on the photographic film and traverse a variable tickness. The latter effect is accounted for, according to Hellner,[10] by the factor $C(0)/C(\mu)$ with $C(\mu)$ given by

$$C(\mu) = 1 - \exp(-k_e \sec \mu) + \exp[-(k_e + k_b) \sec \mu] - \exp[-(2k_e + k_b) \sec \mu] \quad (1)$$

where μ is the angle of incidence on the film of the diffracted beam and k_e, k_b are the products of the mass absorption coefficients and mass per unit area for film emulsion and base, respectively, and were evaluated (counter measurements) from the X-ray absorption of an intact film and of a film with emulsion removed ($k_b = 0.1856$, $k_e = 0.4950$).

The equation for converting the energy per unit area E_{obsd} into diffracted intensity $I_{obsd,i}$ (see Fraser[11]) is, in the case of cylindrical camera,

$$I_{obsd,i} = \frac{E_{obsd}}{\cos^3 \mu} \quad (2)$$

apart from polarization factor (considered later), assuming negligible sample absorption effects and using arbitrary units.

The background intensity due to the incoherent scattering and to the amorphous material was not subtracted ab initio because we have preferred to account for it in the subsequent least-square fitting stage.

As the half-height peak width ranges from 0.5 to 1.2 mm and the bottom width ~1.0 to 2.4 mm (considering the peaks finished when intensity is dropped to 10% of maximum value), the sampling adopted along the layer line (100 μm, see above) allows ~10–24 measurements for each peak which represents a sufficient sampling.

Least-Square Fitting

The whole-pattern structure refinement from fiber diffraction data, based on a least-square (ls) fitting procedure, can be planned out, as already discussed,[1] by comparing the "observed" diffraction intensities $I_{obsd,i}$ with the ones calculated as $I_{calcd,i} = S\sum_k I_k \Omega_{ik}$ where S denotes a scale factor, i any measured point of the diffraction pattern, k any Bragg reflection, I_k the corresponding "calculated" integrated intensity, and Ω_{ik} a normalized two-variable distribution function. An important difference with respect to the ordinary ls refinement method, matching observed and calculated *integrated* intensities I_k instead of *point-by-point* intensities I_i, is that the latter not only depend on structure (as I_k does) but also on the quantities which control Ω_{ik}, i.e.: (i) lattice constants and camera radius R_c (in the case of cylindrical camera); (ii) a number of "profile parameters" which determine the spread-off of intensity in the neighboring Bragg positions.

The first dependence is very strong since the position of diffraction peaks is affected, with the advantage, however, of obeying precise geometrical rules (see Appendix). The second dependence, instead, obeys ill-defined functional forms as discussed later.

As the observed $I_{obsd,i}$ intensities are measured on several films, an equal number of scale factors must be considered. Furthermore it was introduced as "calculated" a contribution $B_{calcd,i}$ for diffuse diffraction (background) expressed by a parametrized function (see later). Introducing also statistical weight factors for taking into account the variability of standard errors of the measurements ($w_i = 1/\sigma_i^2$), the minimized function to be considered is

$$\chi^2 = \sum_i w_i[I_{obsd,i} - I_{calcd,i}]^2 = \sum_i w_i[I_{obsd,i} - S_{n_i}(B_{calcd,i} + \sum_k I_k \Omega_{ik})]^2 \quad (3)$$

where n_i is the film to which the i-th observation belongs.

The least-square fitting procedure has been implemented on the basis of the above relationship (3), considering as variables (i) the scale factors S_{n_i}, (ii) the lattice constants and the effective film bending radius R_c affecting mainly Ω_{ik}, (iii) the profile parameters which also affect Ω_{ik}, (iv) the parameters for expressing the calculated background $B_{calcd,i}$, and (v) the structural parameters and thermal vibration parameters which control the calculated structure factor and hence the calculated I_k.

Since the dependence is nonlinear (except for S_{n_i}), the ls procedure was designed on the basis of the Gauss–Newton method.[12] The program, operating in full-matrix fashion, allows adjusting *simultaneously all type of parameters*.

Structural parameters treated by the program are *not* atomic fractional coordinates. Due to the limited information contained in the fiber spectrum it is necessary to perform *constrained refinement* reducing the number of *independent variables*. To this end we have preferred the approach of using "generalized coordinates" as already done in powder full-pattern refinement[7] so reducing both the size of the working matrix and the number of Lagrange multipliers.

Indeed with this approach also bond lengths are potentially refinable quantities. In the present case, however, they were kept fixed because of the complexity of structure and the scarcity of information. In other cases[13] with more favorable conditions this point will be investigated thoroughly.

In the present case the ls refinement has been carried out by using 28 independent parameters altogether (eight structural) as follows.

Film Bending Radius and Lattice Constants. With data confined to low ϑ values (actually $\vartheta < 38°$), refinement of *both* R_c and lattice constants is unpracticable owing to the very high parameter correlation. We have so adjusted R_c only (also for compesating film-shrinkage effects) using the lattice constants by Mencick as fixed quantities.

Profile Parameters. As already discussed,[1] it is convenient to refer the Ω_{ik} distribution function to a pair of curvilinear film coordinates τ,ρ. The former are the constant-2ϑ lines and the latter the lines orthogonal to the former (see in the Appendix the analytical equations). The shape of the photographic spots in this reference frame is substantially "rectangular" and Ω_{ik} can be assumed symmetrical with respect to the centre of the spot (Bragg position) and factorizable in two one-variable functions:

$$\Omega_{ik} = \Omega(\tau_i - \tau_k, \rho_i - \rho_k) = f_\tau(\tau_i - \tau_k) f_\rho(\rho_i - \rho_k) \quad (4)$$

τ_i, ρ_i being the coordinates of the i-th point and τ_k, ρ_k the Bragg positions for the k-th reflection.

From a previous study[1] Gauss functions were found to be adequate for expressing both f_τ and f_ρ. The normalized expression for f_τ is

$$f_\tau(\tau_i - \tau_k) = \frac{2(\ln 2)^{1/2}}{\pi^{1/2}} \frac{1}{H_\tau} \exp\left[-4 \ln 2 \left(\frac{\tau_i - \tau_k}{H_\tau}\right)^2\right] \quad (5)$$

H_τ being the half-height peak width along τ. For f_ρ the same expression holds with ρ_i, ρ_k, H_ρ replacing τ_i, τ_k, H_τ.

Inspection of the fiber spectra shows, however, that half-height peak widths H_τ and H_ρ are not the same for all reflections but vary regularly with the position on the film of the reflection. The problem of finding appropriate analytical forms for expressing this dependence deserves much attention, but it is better tackled by considering cases with lesser overlap which will be reported elsewhere. At present we have considered the following empirical dependence of H_τ and H_ρ on polar film coordinates τ_k, φ_k of the k-th reflection:

$$H_\tau = H_\tau^0 + \mu_1\gamma_k + \mu_2\varphi_k$$

$$H_\rho = H_\rho^0 + \mu_3\gamma_k + \mu_4\varphi_k \qquad (6)$$

where μ_i are empirical parameters to be adjusted by the ls procedure.

Scale Factors and Thermal Vibration Parameters. Initially the four S_i values were constrained to vary proportionally to film exposures. Subsequently they were released as independent quantities. The isotropic thermal vibration was considered with an unique B_{iso} value according to the factor $\exp(-2B_{iso}\sin^2\vartheta/\lambda^2)$, multiplying the calculated I_k.

Background Parameters. Owing to the presence of nonstereoregular fractions in commercial IPP, the stretched fibers contain some noncrystalline but partially oriented material. As a consequence as pointed out by Leroy et al.[14] diffused scattering is not spherically symmetric, and the halos typical of noncrystalline substances are more intense in the equatorial region of the fiber spectrum. Since the diffraction intensity is modest, an empirical treatment seems to be appropriate. So we have treated the equatorial regions of the fiber pattern and the nonequatorial ones differently. In the former case $B_{calcd,i}$ was evaluated as

$$B_{calcd,i} = B_{halo} + b_5 + b_6 \sin\vartheta \qquad (7)$$

and in the latter case, instead, as

$$B_{calcd,i} = b_7 + b_8 \sin\vartheta \qquad (8)$$

where B_{halo} was expressed by a Gaussian form:

$$B_{halo} = \frac{b_1}{b_2 b_3}\exp\left[-\left(\frac{x_f}{b_3}\right)^2\right]\exp\left[-\left(\frac{y_f - b_4}{b_2}\right)^2\right] \qquad (9)$$

In the above expressions x_f and y_f are the cartesian film coordinates (x is the fiber axis) and b_i are empirical constants. Parameters b_2 and b_3 (y- and x-widths of the equatorial halo) as well as b_4 (center of the halo along y) were drawn from plots of diffused intensity along x, y and kept constant in ls refinement, whereas b_1, b_5, b_6, b_7, and b_8 were also refined during the fit.

Structural Parameters. The early structure assigned to IPP is $C2/c$ by Natta and Corradini[4] (see Figure 2, bottom). Subsequently Mencick found better agreement with a $P2_1/c$ model having, however, some disorder in the orientation of up and down helices[5] (see Figure 2, top). Hikosaka and Seto[15] have shown that a structural transition from a $C2/c$ to a $P2_1/c$ structure takes place during fiber annealing and have proposed a model for the transition itself. More recently Corradini et al.[16] have studied the statistical distribution of chains in the crystalline structure of IPP as a function of thermal treatment and have carried out packing energy calculations so finding, on the basis of Lennard-Jones potential functions, that

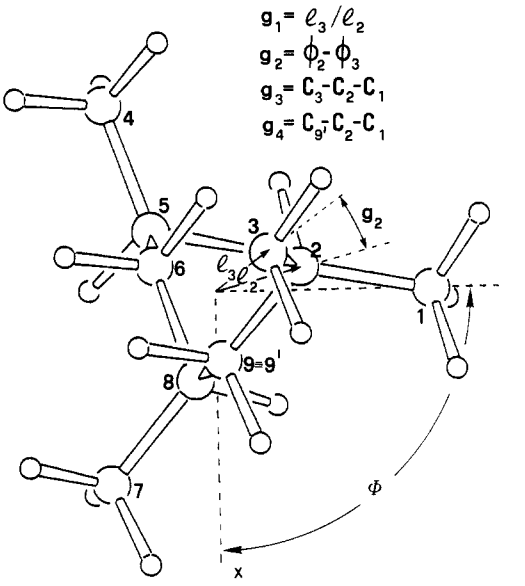

Figure 1. Molecular model for IPP having 3_1 symmetry with arbitrary chain conformation. The definition of gc is indicated.

$P2_1/c$ gives the best packing. These authors have obtained for CH_3 group positions values in agreement with those by Hikosaka and Seto.

In the present work we have carried out least-square fits both with $C2/c$ and $P2_1/c$ space groups within Mencick's model. We have not yet considered the model by Hikosaka and Seto[15] since it requires distinct profile parameters for $(h + k)$ even and odd reflections.

As the present problem suffers from large reflection overlap, it is advantageous to take into account all a priori structural information available. As a matter of fact the C–C bond lengths are certainly foreseeable, while C–C–C bond angles as well as chain torsion angles could deviate appreciably from the canonical values for sp^3 geometry and staggered conformation of C–C bonds. The 3_1 chain symmetry (not retained in the crystal) is also uncertain. To begin with we have thought it important to reduce the number of variables as much as possible and then we have assumed the structural equivalence of the three propylene units belonging to the crystallographic asymmetric unit (a whole turn of 3_1 helix), a customary working hypothesis in linear polymer structure analysis.[18] This restraint could be removed in a future investigation.

In order to include the above information we have adopted a least-square fitting procedure for treating fiber data similar to that illustrated in ref 7 for powder data introducing as structural variables *generalized coordinates* (gc) instead of the usual *positional coordinates* of atoms. The general procedure devised for helices having two kinds of atoms in the chain was adopted[7] which enables the $l_i\phi_i z_i$ cylindrical coordinates of the chain (see Figure 1) to be expressed as a function of four gc (besides b = C–C bond length and c = helix repeat). The gc g_1 and g_2 are defined as $g_1 = l_3/l_2$ and $g_2 = \phi_2 - \phi_3$ (see Figure 1); the gc g_3 and g_4 are the C3–C2–C1 and C9′–C2–C1 bond angles (see details in the Appendix). The crystal structure requires four additional gc, viz., the overall translations $x_0y_0z_0$ and one overall rotation parameter Φ.

The advantage of using g_1 and g_2 instead of more familiar valence and torsion angles is that g_1 and g_2 are *truly independent variables*, whereas the use of 2 + 2 valence and torsion angles would require introducing two Lagrange multipliers to ensure helix continuity. We have preferred to avoid Lagrange multipliers although the ls program implemented by us allows also the use of them.

Table I
Parameters Resulting in the Various Refinements Performed[a]

parameter	A Mencick's $P2_1/c$ (not refd)	B Mencick's $P2_1/c$ (refd)	C Natta's $C2/c$ (refd)
H_r^0, mm	0.475 (13)		
μ_1	0.0384 (8)		
μ_2, mm/rad	0.022 (16)		
H_ρ^0, mm	0.198 (9)		
μ_3	0.0257 (7)		
μ_4, mm/rad	0.198 (12)		
R_c, mm	28.363 (3)	28.334 (3)	28.321 (4)
S_1	0.0584 (9)	0.0603 (8)	0.0633 (10)
S_2	0.187 (2)	0.187 (2)	0.203 (2)
S_3	0.807 (9)	0.694 (8)	0.774 (8)
S_4	2.65 (4)	2.95 (4)	4.06 (5)
B_{iso}, Å^2	2.98 (9)	3.63 (8)	3.05 (10)
f factor	0.936 (3)	0.958 (3)	
b_1	154 (5)	212 (5)	189 (5)
b_2	5.905		
b_3	0.636		
b_4	7.878		
b_5	16.1 (3)	13.9 (3)	9.86 (2)
b_6	−11.6 (5)	−9.4 (4)	−5.2 (3)
b_7	22.8 (3)	19.9 (3)	14.9 (2)
b_8	−25.7 (4)	−22.0 (4)	−16.7 (2)
g_1	0.986	0.920 (5)	1.115 (6)
g_2, deg	118.9	117.8 (3)	110.6 (3)
$g_3 = g_4$, deg	108.7	108.2 (2)	108.6 (2)
x_0, Å	$a \sin \beta/4$	1.639 (3)	0.225 (2)
y_0, Å	7.923	7.798 (2)	2.547 (3)
z_0, Å	−0.030	0.276 (3)	1.383 (4)
Φ, deg	88.0	85.3 (1)	−96.8 (1)
C2–C3–C5, deg	114.7	116.9	113.9
C9′–C2–C3, deg	114.0	112.4	120.0
C3–C2–C9–C8, deg	178.9	178.0	169.9
C5–C3–C2–C9, deg	−59.6	−59.2	−55.7
R_1	0.206	0.214	0.239
R_2	0.320	0.344	0.369
R_3	0.308	0.267	0.317
R_4	0.140	0.124	0.145

[a] Standard errors (in parentheses) are those resulting from the diagonal terms of the inverted normal matrix.[11] The meaning of g_i is given in Figure 1. The four disagreement R indices (referred to the four films of different exposures) are defined as $\sum_i |I_{obsd,i} - I_{calcd,i}| / \sum_i I_{obsd,i}$. Lattice constants used are (Mencick[5]) a = 6.63, b = 20.78, c = 6.50 Å, β = 99.50°.

According to Mencick, IPP helices are disposed in the $P2_1/c$ unit cell with some disorder: in each site there is a fraction f of *up* helices and a fraction $1 - f$ of *down* helices having the same chirality, related to each other through the noncrystallographic operator $^1/_2 - x, y, ^1/_2 - z$ and both having $x_0 = a \sin \beta/4$. The f factor itself is, in Mencick's model, a structural variable and has been refined.

Fitting of the Different Models and Comparisons

First, considering the structural parameters by Mencick[5] as fixed, we have adjusted the effective film bending radius R_c, background parameters, overall isotropic thermal factor, scale factors, profile parameters, and the f factor. The latter, set initially to f = 0.75 according Mencick, was waived because it depends on mechanical and thermal treatments and is presumably different from sample to sample. After convergence (in a few cycles shifts become a small fraction of standard errors) the values listed in Table I, column A, were obtained. The corresponding plot of observed and calculated intensities is shown in Figure 3.

The structural parameters were then released, *within Mencick's model*, by waiving, however, the $x_0 = a \sin \beta/4$ condition (this detail has a negligible effect) and keeping the profile parameters constant. The values so obtained are those listed in Table I, column B, and the corresponding atomic fractional coordinates are those listed in Table II. The improvement of fit is evident on inspection of the plot of observed-to-calculated intensities shown in Figure 3, while the R indices decrease appreciably only for

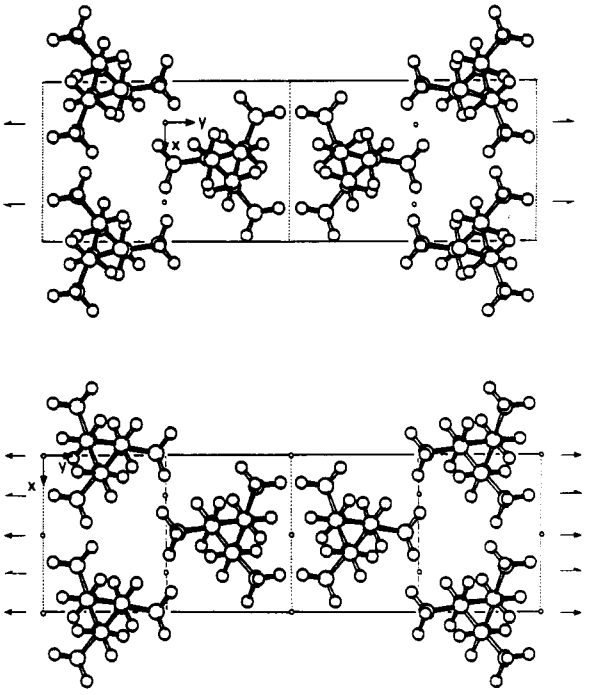

Figure 2. Crystal structures for IPP top is shown by the $P2_1/c$ structure, bottom by the $C2/c$ structure.

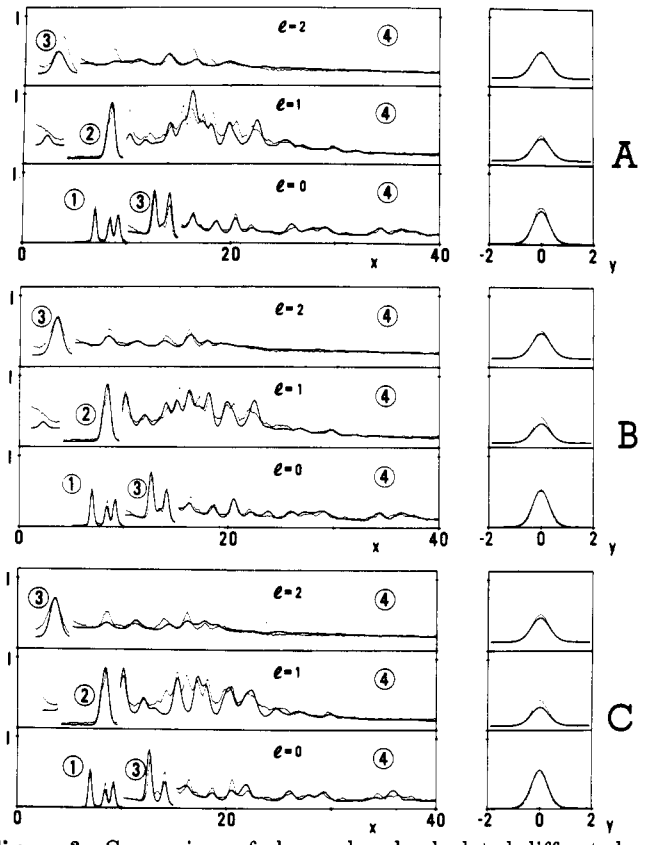

Figure 3. Comparison of observed and calculated diffracted intensities at the end of refinements A, B, and C. Thick lines refer to calculated and thin lines to observed intensities. The left plots indicate sections along the layer lines of the diffraction pattern (y, mm), the right plot sections across the layer lines (x, mm) for the strongest equatorial peaks only. Diffracted intensities are plotted in arbitrary units and the film number is also indicated (circled).

Table II
Atomic Fractional Coordinates x/a, y/b, and z/c and Their Standard Errors Resulting from B and C Refinements[a]

atom	x/a	y/b	z/c
	Fit B		
C4	−0.0611 (6)	0.3287 (2)	−0.0098 (5)
C5	0.1592 (5)	0.3458 (2)	0.0903 (10)
C6	0.1699 (6)	0.3472 (2)	0.3286 (9)
C7	0.5346 (10)	0.3136 (4)	0.4237 (9)
C8	0.3772 (6)	0.3650 (2)	0.4603 (9)
C9	0.3680 (6)	0.3672 (2)	0.6952 (10)
C1	0.2783 (14)	0.4835 (2)	0.7139 (11)
C2	0.2154 (6)	0.4148 (1)	0.7664 (10)
C3	0.2139 (7)	0.4112 (2)	1.0026 (10)
	Fit C		
C4	−0.0727 (8)	0.2291 (3)	0.2004 (6)
C5	−0.0765 (8)	0.1592 (2)	0.2788 (14)
C6	−0.1021 (9)	0.1602 (2)	0.5098 (14)
C7	−0.3087 (13)	0.0589 (5)	0.4941 (12)
C8	−0.1146 (6)	0.0928 (2)	0.6057 (13)
C9	−0.1044 (9)	0.0854 (2)	0.8428 (12)
C1	0.2775 (11)	0.0797 (6)	0.9260 (13)
C2	0.0872 (6)	0.1156 (2)	0.9730 (13)
C3	0.1026 (6)	0.1221 (3)	1.2109 (14)

[a] The listed coordinates are those corresponding to the parameters given in Table I, columns B and C. For atom labeling see Figure 1. Standard errors are given in parentheses and are those computed from the final inverted normal matrix according to the usual procedures.[11]

long-exposure data. The f values obtained, both with Mencick's coordinates fixed ($f = 0.936$) and after structure adjustment ($f = 0.958$), are closer to unity than Mencick's value ($f = 0.75$). Some refinement runs performed by initially setting f to lower values (e.g., $f = 0.55$) give rise to the same result. In our opinion, however, the unlikeness of "disorder" parameter f (surely related to the thermal and mechanical history of the samples) has not a clearcut physical significance and two-phase structural models (to be considered in the future with improved algorithms) are more appropriate for this purpose.

As concerns the reliability of the resulting structural parameters, the following considerations apply:

(i) All C–C–C bond angles converge to reliable values, in particular the CH–CH_2–CH chain angle (116.9°) is comparable with the ones observed in proper low molecular weight model compounds.[19,20]

(ii) The z_0 parameter (overall helix-translation) is appreciably different from Mencick's value (+0.30 Å) and close to the Hikosaka and Seto value (+0.13 Å). Some refinement runs carried out by giving initially z_0 parameter values ranging from −0.25 to +0.74 Å gave the same final result.

(iii) The isotropic thermal parameter B_{iso} converges to a rather small value if compared to values obtained in structural analyses based on "integrated" intensities. It is worthwhile recalling that low-temperature parameters (also negative values!) are usually observed in powder whole-pattern studies.[21]

(iv) The standard errors of adjusted parameters listed in Tables I and II are those computed with usual algorithms[12] from the diagonal terms of the inverted normal matrix. These values are presumably underestimated similarly to what occurs in whole-pattern powder profile analyses.[21]

The structure refinement within the $C2/c$ model was then carried out starting from the same chain model as Mencick, but assuming the CH_3 z positions of Hikosaka and Seto.[14] The convergence values obtained are those given in Table I, column C. The fit is decidedly worse on inspection of the observed-to-calculated intensity plot (see Figure 3), on examination of the disagreement of R indices, and on considering the resulting values of bond and torsion angles.

Conclusions

The present study, the first example of a fiber whole-pattern structure refinement, does not claim to give new and ultimate answers to the intriguing problem of the helix statistics in the IPP structure, because an exhaustive study should begin with a careful characterization of the used material (molecular weight and steric purity) and be based on examination of several samples (not a single sample!) with well-standardized thermal and mechanical treatments. It seems to us, however, that two positive results have been obtained. The first is that of yielding a structural model for the IPP helix through an *authentic refinement*, with the only assumption being that of known bond legths and 3_1 symmetry. The second, the most important one in our opinion, is that the reliable chain structure obtained demonstrates the feasibility of the fiber whole-pattern approach, also under unfavorable conditions for high reflection overlap, scarcity of data, and structural disorder.

There are of course a number of points deserving closer attention, viz. (i) the treatment of background intensity, (ii) the adoption of a less arbitrary functional form for expressing the dependence of peak widths on film position, and (iii) a correction for compensating possible misalignment. Furthermore, the choice of film coordinates as the "variables" for expressing the two-dimensional profile functions could be also revised by selecting, for instance, the reciprocal space coordinates. These points and others will be the objects of future studies, and it is our purpose to select more favorable structures having possibly a higher number of observable Bragg reflections, sharper peaks, and less peak overlap.

Acknowledgment. We are grateful to Professors P. Corradini and V. Petraccone for a fiber sample and for some discussions and criticism. We are also indebted to Prof. G. Zannotti, Università di Padova, for the use of an Optronics photoscan instrument and for useful discussions. Financial support by Ministero della Pubblica Istruzione is also acknowledged.

Appendix

Working Formulas for Calculating $I_{calcd,i}$. For carrying out the ls refinement based on minimization of χ^2 given in (3), I_{calcd} is calculated as

$$I_{calcd,i} = S_{n_i}(B_{calcd,i} + \sum_k I_k \Omega_{ik}) \tag{10}$$

where i denotes a single *point* of diffraction pattern and k a single *reflection*.

S_{n_i} (scale factors) and $B_{calcd,i}$ (diffused intensity) have been discussed in the text. For I_k the equation holds

$$I_k = m_k L_k p_k F_k^2 \tag{11}$$

where m_k is the multiplicity factor, $L_k = (\sin^2 2\vartheta_k - \zeta_k^2)^{-1}$ is the Lorentz factor (ζ_k is the component of the scattering vector of length 2 sin ϑ_k along the fiber axis), $p_k = {}^1/_2(1 + \cos^2 2\vartheta_j)$ is the polarization factor and F_k is the calculated structure factor. p_k and L_k depend very weakly on lattice constants while F_k depends fundamentally on *structure*.

Ω_{ik} is expressed according to (4) and (5) and so depends strongly on lattice constants and camera radius R_c as the latter affect τ_k, ρ_k for each reflection. The *curvilinear* film coordinates τ, ρ are evaluable from the *Cartesian* coor-

dinates x,y through the equations

$$\tau = \int_{u=0}^{u=x/R_c} \left[1 + \frac{u^2}{(1+u^2)(\tan^2 2\vartheta - u^2)} \right]^{1/2} du \quad (12a)$$

$$\rho = \int_{u=0}^{u=1} \left[1 + \frac{w^2(u)}{1-w^2(u)} \left(\frac{xu}{R_c} + \frac{R_c}{xu} \right)^2 \right]^{1/2} du \quad (12b)$$

where the function $w(u)$ is

$$w(u) = u \sin\left(\frac{y}{R_c}\right) \exp\left[(u^2-1)\frac{x^2}{2R_c} \right] \quad (13)$$

Calculation of Crystallographic Coordinates from the Generalized Coordinates. Crystallographic coordinates (see Figure 1) can be obtained from the gc and the parameters b = C–C bond length and c = helix repeat (i.e., lattice c constant) as follows:

(i) evaluation of cylindrical coordinates l, ϕ, z for C2 and C3 atoms ($\phi_2 = 0$, $z_2 = 0$ by definition),

$$q_1 = \cos g_2 - \cos(\tfrac{2}{3}\pi - g_2) \quad (14a)$$

$$q_2 = \left(b^2 - \frac{c^2}{36} \right) \frac{c^2}{9{g_1}^2 q_1} \quad (14b)$$

$$q_3 = \frac{c^2}{18{g_1}^2 q_1}(1 + {g_1}^2 - 2g_1 \cos g_2 + g_1 q_1) \quad (14c)$$

$$l_2 = [(q_2 + {q_3}^2)^{1/2} - q_3]^{1/2} \qquad l_3 = l_2 g_1 \quad (14d)$$

$$\phi_2 = 0 \qquad \phi_3 = -g_2 \quad (14e)$$

$$z_2 = 0 \qquad z_3 = \frac{c}{6} + \frac{3 l_2 l_3 q_1}{c} \quad (14f)$$

(ii) definition of the positions of other carbon atoms of the chain C5, C6, C8, and C9 by applying the 3_1 screw operator twice; (iii) definition of the positions of the methyl side groups C1 by intersection of the cone of axis C9′–C2 and aperture $\pi - g_4$ with the cone of axis C3–C2 and aperture $\pi - g_3$ (the choice between the two possible solutions is a matter of chirality), a similar construction applies to C4 and C7 atoms; (iv) change of the origin making $z_1 = 0$ and $\phi_1 = 0$; (v) rotation of Φ of the whole helix and translation of x_0, y_0, z_0.

In the evaluation of I_{calcd} hydrogen atoms were also considered by placing them according the ideal sp^3 geometry for carbon atoms and staggered conformations for methyl groups.

Registry No. IPP, 25085-53-4.

References and Notes

(1) Immirzi, A.; Iannelli, P. *Gazz. Chim. Ital.* **1987**, *117*, 201.
(2) Rietveld, H. M. *Acta Crystallogr.* **1967**, *22*, 151.
(3) Rietveld, H. M. *J. Appl. Crystallogr.* **1969**, *2*, 65.
(4) Natta, G.; Corradini, P. *Nuovo Cimento* **1960**, Suppl. 15, 40.
(5) Mencick, Z. J. *Macromol. Sci. Phys.* **1972**, *6*, 101.
(6) Immirzi, A. *Acta Crystallogr., Sect. A* **1978**, *A34*, S348.
(7) Immirzi, A. *Acta Crystallogr., Sect. B* **1980**, *B36*, 2378.
(8) Immirzi, A. *Gazz. Chim. Ital.* **1980**, *110*, 381.
(9) Immirzi, A.; Porzio, W. *Acta Crystallogr., Sect. B* **1982**, *B38*, 2788.
(10) Hellner, E. Z. *Kristallografiya* **1954**, *106*, 122.
(11) Fraser, R. D. B.; Macrae, T. P.; Miller, A.; Rowlands, R. J. *J. Appl. Crystallogr.* **1976**, *9*, 81.
(12) Ortega, J. M.; Reinholdt, W. C. *Iterative Solution of Nonlinear Equations in Several Variables*; Academic: New York, 1970.
(13) Iannelli, P.; Immirzi, A. *Acta Crystallogr., Sect. A* **1987**, *A43*, C-199. (A full paper was submitted to Macromolecules.)
(14) Leroy, B.; Alexander, E.; Michalik, E. R. *Acta Crystallogr.* **1959**, *12*, 105.
(15) Hikosaka, M.; Seto, T. *Polym. J.* **1973**, *5*, 111.
(16) Corradini, P.; Giunchi, S.; Petraccone, V.; Pirozzi, B.; Vidal, H. M. *Gazz. Chim. Ital.* **1980**, *110*, 413.
(17) Corradini, P.; Petraccone, V.; Pirozzi, B. *Eur. Polym. J.* **1983**, *19*, 299.
(18) Corradini, P. In *Stereochemistry of Macromolecules*; Kettley, K., Eds.; M. Dekker: New York, 1968; Vol III, p 1.
(19) Benedetti, E.; Pedone, C.; Allegra, G. *Macromolecules* **1970**, *3*, 16.
(20) Bocelli, G.; Grenier-Loustalot, M. F. *Acta Crystallogr. Sect. C* **1983**, *C39*, 636.
(21) Albinati, A.; Willis, B. T. M. *J. Appl. Crystallogr.* **1982**, *15*, 361.
(22) Bürger, M. J. *X-ray Crystallography*; Wiley: New York, 1965.

Excluded-Volume Effects in Rubber Elasticity. 3. Segment Orientation[1]

J. Gao and J. H. Weiner*

Department of Physics and Division of Engineering, Brown University, Providence, Rhode Island 02912.

Received August 3, 1987; Revised Manuscript Received September 8, 1987

ABSTRACT: The effect of excluded volume on segment orientation in rubber elasticity is studied by molecular dynamics simulation of model systems of freely jointed chains with a truncated Lennard-Jones repulsive potential acting between all atoms. In a single chain with fixed end-to-end distance L and periodic boundary conditions, it is found that excluded volume causes negative orientation ($\langle P_2 \rangle < 0$) for sufficiently small L. This effect has been observed previously for a tie molecule and suggests an analogy between the confining effect of the crystalline lamellae on the tie molecule and that of excluded volume on the chain with periodic boundary conditions. In a system of three chains, corresponding to the three-chain model of rubber elasticity, it is found that intrachain excluded-volume interactions alone cause a decrease in orientation in the tensile region, but inter- and intrachain interactions together cause an increase in orientation beyond the ideal chain case. It is also found that excluded volume has a much greater effect upon the chains with end-to-end vector perpendicular to the elongation direction than upon the chain parallel to that direction.

Introduction

A rubberlike solid represents, from the atomistic viewpoint, a rather complex system. The topological character of the covalent bonds which form the long-chain molecules permits large-amplitude thermal motion of their atoms, as in a liquid, while cross-linking of these molecules supports the types of deformation characteristic of a solid. There are, in addition, noncovalent interactions between

0024-9297/88/2221-0773$01.50/0